

## Magneto-rotational Instability in Core-Collapse Supernovae

T. Rembiasz<sup>1</sup>, M. Obergaulinger<sup>2</sup>, P. Cerdá-Durán<sup>2</sup>, E. Müller<sup>1</sup>, M. Angel Aloy<sup>2</sup>

<sup>1</sup> Max-Planck-Institut für Astrophysik, Garching, Germany

<sup>2</sup> Universitat de València, Valencia, Spain

The influence of magnetic fields is one of the major uncertainties in the explosion mechanism of core-collapse supernovae. Only very strong magnetic fields, which are in equipartition with the kinetic energy density, i.e., of the order of  $10^{15}$  G, can play a dynamically important role. According to state-of-the-art stellar evolution theory, the strongest magnetic fields of typical supernova progenitors (massive stars) are unlikely to exceed  $10^9$  G (Heger et al. [6]). Therefore, it is important to investigate whether and how the initial magnetic fields could be amplified by  $5 \sim 6$  orders of magnitude during a supernova explosion.

The collapse to a proto-neutron star compresses the magnetic field frozen into the infalling gas because of the high conductivity of degenerate stellar matter and amplifies it by roughly 3 orders of magnitude. After the collapse, further amplification can be provided by hydrodynamic instabilities such as convection or the standing accretion shock instability. If the core rotates, a poloidal field will be wound up into a toroidal component in a process that increases the magnetic field strength linearly in time. However, this mechanism is insufficient on the explosion timescale for the rotation rates currently predicted by stellar evolution calculations for the iron cores of the progenitor stars. Additionally, the magneto-rotational instability (MRI; see, e.g., Balbus & Hawley [2]), because of its exponential growth, might amplify even a weak seed field to a dynamically relevant strength very rapidly (Akiyama et al. [1]).

The MRI has been studied intensively in accretion disks where it excites turbulence and provides the effective viscosity required for the accretion of the gas. Nevertheless, the saturation level of

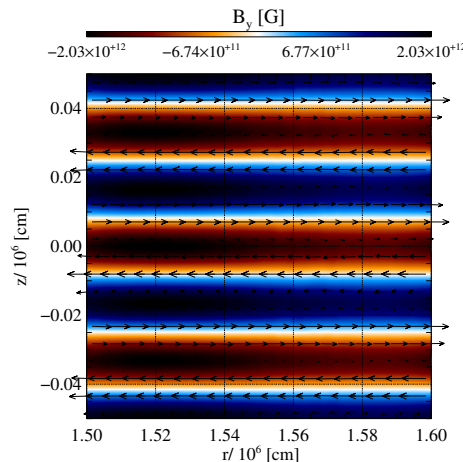


Figure 1: Toroidal magnetic field component  $B_\phi$  (colour) and fluid velocity projection on the  $rz$  plane (black arrows) 5 ms after introducing random velocity perturbations to the system.  $B_\phi$  (also  $B_r$ ) forms anti-parallel MRI channels, which are tearing mode unstable.  $v_r$  forms shear layers, which can be destroyed by the Kelvin-Helmholtz instability.

the instability is still not fully understood.

Though previous simulations (Obergaulinger et al., [7]) we have confirmed that the growth rates are sufficiently high for the MRI to present a viable amplification mechanism, it is still unclear whether MRI-driven field growth over many orders of magnitude is indeed possible. This uncertainty is due to our lack of understanding of the physics of the termination of MRI growth and the subsequent non-linear turbulent phase. The early phase of the MRI is characterized by coherent laminar flows (channel modes, see Fig. 1), which are unstable against secondary, parasitic instabilities (Goodman & Xu [5]) driven by the flow (Kelvin-Helmholtz (KH)) or the current (tearing modes (TM) (Furth et al., [4])). When these parasites disrupt the channel modes, the growth of the MRI terminates. Based on theoretical analysis, Pessah [8] suggested that the saturation level of MRI-driven turbulence and therefore the final magnetic field strength can be estimated by a study of the parasitic instabilities.

We want to test this hypothesis in direct numerical simulations (see our results from a simulation in Fig. 2). The properties of the MRI, its parasites and MRI-driven turbulence are affected by viscosity and resistivity. To study these dependencies in detail, we extend our previous set of simulations to study the interplay between the MRI and the parasites in three-dimensional, non-ideal MHD simulations.

We use a grid based flux-conservative finite-volume MHD code *Aenus* (Obergaulinger et al in prep). In order to prevent the spurious development of a non-zero divergence of the magnetic field, the code exploits the constrained-transport discretisation of the MHD equations (Evans & Hawley [3]). It further uses high-resolution shock-capturing methods based on high-order methods for the reconstruction (monotonicity-preserving schemes, Suresh & Huynh [9]) of the conserved variables and multi-stage (MUSTA; Titarev & Toro [10]) approximate

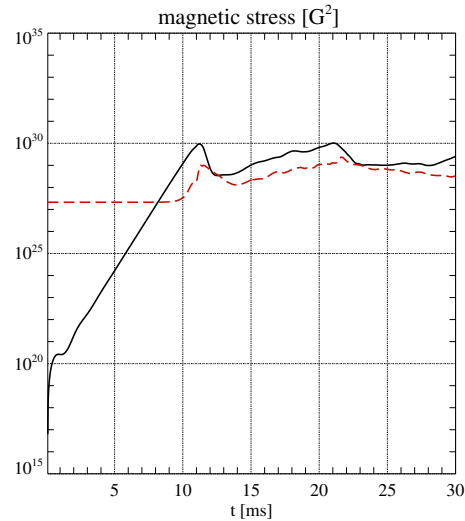


Figure 2: Time evolution of volume averaged  $|B_r B_\phi|$  (solid black) and  $|B_z B_z|$  (red dashed) Maxwell stress components.

The component  $|B_r B_\phi|$ , growing exponentially until  $t \approx 10\text{ms}$ , is a direct measure for the MRI amplitude. For  $t > 10\text{ms}$  the  $|B_z B_z|$  component, which is an indicator for the growth of the parasitic instabilities, starts to grow faster than MRI. At that point, the MRI stops to grow, and the model enters the turbulent saturation phase during which the stress oscillates around a roughly constant level.

Riemann solvers: Lax-Friedrich (LF), Harten-Lax-van Leer (HLL) and Harten-Lax-van Leer-Discontinuities (HLLD).

Since the MRI wavelength is of order of meters, one cannot resolve it properly in global core-collapse supernova simulations. Therefore, we run 3D simulations in a shearing box of the size  $1\text{km} \times 4\text{km} \times 1\text{km}$ , which is placed 15 km from the center of a proto-neutron star. We choose different values of initial magnetic field, resistivity and viscosity. For each simulation we want to identify which parasitic instability caused the termination of the MRI growth.

To gain a better understanding of the parasitic modes, we study them in detail in auxiliary simulations. We simulate the evolution of TM-unstable current sheets (see Fig. 3) and KH-unstable shear layers and determine the growth rates of the instabilities as a function of initial magnetic field, shear velocity, resistivity and viscosity. We compare the results to the theoretically known dispersion relations of both instabilities. One of the main consequences of the comparison is a detailed understanding of the numerical viscosity and resistivity of our code. These are crucial inputs for performing 3D MRI simulations because we need to ensure that the physical viscosity and resistivity exceed the numerical ones in each case.

Our final goal is the formulation of a simple model connecting the initial magnetic field, and the resistivity and viscosity of the matter with the termination and saturation of the MRI.

## References

- [1] Akiyama, S., Wheeler, J. C., Meier, D. L. & Lichtenstadt, I. 2003, *ApJ*, **584**, 954
- [2] Balbus, S. A. & Hawley, J. F. 1998, *Reviews of Modern Physics*, **70**, 1
- [3] Evans, C. R. & Hawley, J. F. 1988, *ApJ*, **332**, 659
- [4] Furth H.P., Killeen J., Rosenbluth M.N., 1963, *PhFl*, **6**, 459
- [5] Goodman, J. & Xu, G. 1994, *ApJ*, **432**, 213

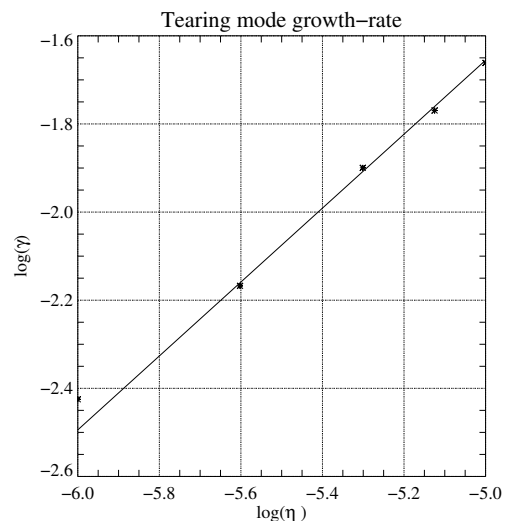


Figure 3: Growth-rate ( $\gamma$ ) of the tearing modes as a function of resistivity ( $\eta$ ). The solid line is a theoretical prediction from Furth et al. [4] and asterisks represent measurements from our simulations. The tearing modes were well resolved and the physical resistivity was much higher than the numerical resistivity of the code.

- [6] Heger, A., Woosley, S. E. & Spruit, H. C. 2005, *ApJ*, **626**, 350
- [7] Obergaulinger, M., Cerdá-Durán, P., Müller, E. & Aloy, M. A. 2009, *A&A*, **498**, 241
- [8] Pessah, M. E. 2010, *ApJ*, **716**, 1012
- [9] Suresh, A. & Huynh, H. 1997, *J. Comput. Phys.*, **136**, 83
- [10] Toro, E. F. & Titarev, V. A. 2006, *J. Comput. Phys.*, **216**, 403